

OF-VO: Efficient Navigation among Pedestrians Using Commodity Sensors

Jing Liang, Yi-Ling Qiao, Tianrui Guan and Dinesh Manocha

Abstract—We present a modified velocity-obstacle (VO) algorithm that uses probabilistic partial observations of the environment to compute velocities and navigate a robot to a target. Our system uses commodity visual sensors, including a mono-camera and a 2D Lidar, to explicitly predict the velocities and positions of surrounding obstacles through optical flow estimation, object detection, and sensor fusion. A key aspect of our work is coupling the perception (OF: optical flow) and planning (VO) components for reliable navigation. Overall, our OF-VO algorithm using learning-based perception and model-based planning methods offers better performance than prior algorithms in terms of navigation time and success rate of collision avoidance. Our method also provides bounds on the probabilistic collision avoidance algorithm. We highlight the realtime performance of OF-VO on a Turtlebot navigating among pedestrians in both simulated and real-world scenes. A demo video is available at <https://gamma.umd.edu/ofvo/>

I. INTRODUCTION

Mobile robots are currently deployed in a wide range of scenarios, including warehouses, airports, malls, and offices [1]. In these indoor and outdoor spaces, robots are used to perform routine tasks such as delivering goods or guiding customers. The ability to perform reliable navigation and avoid collisions with pedestrians and other obstacles is important to perform these tasks.

There are extensive works on robot navigation and collision-avoidance in dynamic scenes [2], [3]. These include model-based techniques based on velocity obstacles [4] and dynamic constraints [2]. However, these methods assume accurate detection or representation of obstacles in the environment [4], [2]. Other techniques have been proposed for dynamic scenes [3], [5], but their performances vary in different environments and none of them are robust enough for all general scenarios [6].

Recently, a number of learning-based approaches have been proposed to perform robot navigation and collision avoidance [7], [8], [9]. These algorithms can handle sensor noise in many scenarios. However, it is challenging to predict the performance in new or unknown scenes with those learning-based models because their performance is governed by the training data. Some model-based navigation algorithms [10], [11] use probabilistic techniques to handle sensor errors, but they are not robust in terms of handling partial observations.

Main Results: We present a novel hybrid scheme for safe navigation of a mobile robot among pedestrians and other obstacles. Our approach takes advantage of learning-based methods to handle sensor data (perception) and a model-based formulation (planning) to compute safe velocities for collision avoidance. Instead of developing an end-to-end



Fig. 1. Navigation among pedestrians in an indoor scene: We highlight the scene captured using a commodity camera mounted on the robot. The image on the left shows the segmentation of pedestrians with colored optical flow computed by our perception algorithm. Blue and red arrows correspond to pedestrian velocities. The curved black arrow represents the robot's trajectory computed using our probabilistic collision avoidance algorithm. The image on the right highlights the environment in which the robot navigates among the pedestrians.

learning pipeline, we use separate components for perception and planning to provide guarantees of collision avoidance. The novel components of our approach include:

- We integrate a segmentation and an optical flow estimation network to detect obstacles. The state-of-the-art pretrained models helps robots perceive the environment accurately in real time.
- We present a modified velocity-obstacle algorithm to perform local navigation and collision avoidance based on partial observations. We highlight improvements over prior velocity obstacle methods and show that our approach is more robust.
- We present bounds for our probabilistic collision avoidance. These bounds provide better guarantee and interpretability than learning-based navigation schemes.

We have tested our algorithm on a Turtlebot robot with commodity sensors, including an Orbecc Astra RGB camera (around \$100) and a 2-D Hokuyo Lidar (costing around \$1000). We have evaluated OF-VO in simulated environments with multiple pedestrians, including high-density cases with more than 10 pedestrians in $5 \times 5 m^2$ area. We used different methods to simulate pedestrian movements, including socially acceptable collision avoidance [12], [13]. Moreover, we tested the algorithm in our laboratory with pedestrians close to the robot and moving in different patterns. Results will be shown in the video. We compared our approach with prior model-based methods like DWA [2] and deep-reinforcement learning algorithms like [14]. We observe 2 – 5X improvement in success rate (and reliability).

II. BACKGROUND AND RELATED WORK

In this section, we briefly survey related work on local navigation and collision avoidance. We also give an overview of prior techniques used in computer vision for object segmentation and motion detection.

A. Collision Avoidance

Many researchers have proposed learning-based algorithms for collision avoidance in real-world scenarios. [15] uses POMDPs to navigate robots in uncertain scenarios. [8] and [9] use deep learning to train end-to-end networks for indoor scenarios. These methods have shown good performance in terms of avoiding static obstacles. However, these methods may not work well in complex dynamic scenes, especially when the pedestrians are moving at different speeds. In addition to considering the uncertainties of perception module, our approach also takes into account different velocities of pedestrians.

Many model-based algorithms [4], [2], [16] have been proposed for motion planning in dynamic scenarios. However, these methods assume accurate detection, localization or representation of obstacles. In real-world scenarios, perception methods tend to be inaccurate due to sensor noise and environment complexity [17]. To address the inaccuracies, [18] proposes a time-to-collision algorithm for reciprocal collision avoidance, though it is mainly limited to simulated scenarios. [19] uses a receding horizon control algorithm with different constraints to navigate robots in uncertain environments. However, this approach can be time-consuming as the algorithm needs to compute several consecutive actions in one step. [10], [17], [20] use velocity obstacles for collision avoidance. However, these methods assume complete observations of nearby obstacles and environments. We also take into account the kinematic constraint of robot and apply the constraint in the velocity space. Overall, our approach results in improved navigation behavior.

Neural networks techniques have been used for navigation with real-world sensors. For example, cameras and Lidar are widely used as inputs to networks in reinforcement learning approaches. For RGB cameras, [21] uses deep double-Q and [22] uses the A3C algorithm to train the policies in cluttered scenarios. [14] uses 2D Lidar along with the PPO algorithm [23] to navigate multiple robots in scenarios with static and dynamic obstacles. Some deep reinforcement learning-based navigation algorithms use a combination of cameras and 2D Lidar [7]. [24] uses inverse reinforcement learning to imitate the behavior of people in crowds. However, these methods can result in oscillation or freezing issues during navigation. Furthermore, it is difficult for these learning-based approaches to provide strong guarantees on collision avoidance in general or arbitrary scenarios. In contrast, our approach only uses learning based methods in the perception module and can provide probabilistic bounds on collision avoidance and navigation.

B. Motion Estimation

Estimating the positions and velocities of moving objects plays an important role in perception tasks. Previous works estimate velocities through trajectory tracking and prediction [25], [7]. Tracking methods can exhibit higher accuracy when the pedestrian is fully contained in the field-of-view of the cameras. However, when a moving pedestrian is very close to the robot, it may be only partially visible, and the

tracking algorithms might fail due to the loss of tracking or mismatch across frames [26]. Instead, we use an optical flow network, which is more robust and the network encodes the movement of objects in pixel-level correspondence. To extract the velocities of objects, our perception approach consists of two modules: optical flow estimation and object detection (see Fig. 2).

Optical flow (OF) is the displacement of the pixel position between two consecutive images. Sparse OF only computes the flow on some landmark points, which takes less time. For real-time performance, other methods [27], [28] use sparse OF to avoid collisions. They use the property that pixels from closer objects tend to move faster, and thus the robot steers to the side with smaller optical flow. Although this rule seems direct and intuitive, the underlying assumption may not hold in complex dynamics scenes. Recently, [29] augments segmentation using optical flow estimation. [30] estimates velocity based on optical flow estimation, but does not perform any segmentation computations. Our estimation using dense segmentation and optical flow is more accurate than prior methods. Traditional dense optical flow estimation can be achieved by optimization with smoothness constraints [31], which takes several minutes to compute on a single image pair. Some learning-based methods based on neural networks [32], [33], [34], [34] have also been designed to estimate the optical flow with accuracy comparable to traditional methods, while running an order of magnitude faster. However, they do not provide accurate average velocity for each moving object, given the fact that different parts of one object may have different velocities. In order to achieve a high accuracy in velocities prediction, we use the state-of-the-art models MaskRCNN [35] and FlowNet2 [33] to calculate the average speed of objects. Our pipeline does not restrict the choices of networks and our current implementation uses these two networks because they are widely used in computer vision. MaskRCNN is implemented in most open-source object detection frameworks [36], [37]. FlowNet2 is one of the most popular methods for optical flow estimation. These two networks are trained on a large volume of data. We use them in simulated environments as well as real-world scenarios.

Lidar sensors can exhibit good performance in terms of computing distances [38], and cameras are widely used for detection estimation [39]. The combination of these two sensors has been used for navigation and autonomous driving [40]. In our method, we fuse the 2D data from Lidar and the images from cameras to compute the obstacles' relative positions and improve the velocity prediction.

III. OVERVIEW

Our approach is designed for non-holonomic robots, whose movement is governed by linear and angular velocities. During each timestep, the robot knows the relative position of its target/goal and needs to navigate to the target in an environment that consists of static and dynamic obstacles. Each obstacle has a velocity \mathbf{v}_i at position \mathbf{p}_i . We do not assume that the dynamic obstacles like the pedestrians

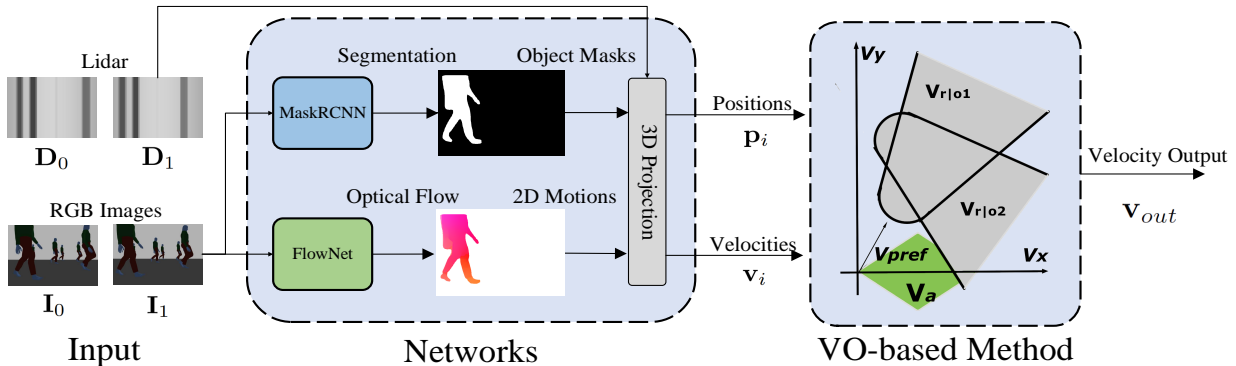


Fig. 2. OF-VO Pipeline: During each time step, our method first takes as input a pair of RGB images and Lidar sequences. The optical flow and segmentation masks are computed using FlowNet and MaskRCNN, respectively. Using Lidar data and intrinsic camera parameters, our 3D projection module computes the positions and velocities from the masks and optical flow. Due to the limitation of the camera’s FOV, 2D Lidar data is also collected to enhance the position estimation. Our method uses a modified velocity obstacles approach to compute a collision-free velocity for the robot that accounts for sensor errors. Before sending the control signals to the robot, a differential driving formulation is used to satisfy the kinematic constraints of the robot.

would completely avoid the robot and design an appropriate navigation scheme. Due to sensor errors, the velocity and the position values may have some uncertainty. In each time step, the robot observes two consecutive RGB and Lidar frames. Images are used by MaskRCNN and FlowNet and then fused with Lidar data to predict the velocities and positions of the moving objects (usually pedestrians) in the scene. The predicted positions and velocities are used in our probabilistic collision avoidance algorithm for local navigation. Figure 2 shows the workflow of OF-VO.

We compute the velocities and positions of surrounding obstacles from Lidar data and RGB images with the help of optical flow estimation and object detection. After that, noises from the perception models are explicitly analyzed and used to improve the overall accuracy of our approach. With the position and velocities, \mathbf{p}_o , \mathbf{v}_o , of detected obstacles, our method uses a modified VO-based algorithm to navigate the robot.

Real-world scenarios inevitably have inaccuracies, occlusions, and only partial observations from the environment due to limited field-of-view. For all obstacles detected by the perception model, we model the inaccuracies in detection as Gaussian distributions. We also provide a lower bound on the confidence of collision avoidance. For unobserved or partially observed objects, we apply non-holonomic kinematic constraints to estimate the feasible velocity space of the robot, as described in Section V. Our integrated approach consists of two parts, learning-based perception and model-based collision avoidance, which are strongly coupled. The hyperparameters in the VO algorithm are chosen according to different bounds on robots’ velocities and different requirements in terms of confidence in probabilistic collision avoidance.

IV. PERCEPTION

In our approach, we use two commodity visual sensors: an RGB camera and a 2D Hokuyo Lidar. We choose to use these two commodity sensors because the RGB camera is good at perceiving detailed information in the scene, while a 2D Lidar can accurately detect distances of nearby objects.

The input to our perception module is a pair of consecutive RGB frames and Lidar data, and the output is the estimated positions \mathbf{p}_o and velocities \mathbf{v}_o of the nearby obstacles. Our algorithm builds on recent learning-based computer vision methods. We use an optical flow network FlowNet [33] and a segmentation network MaskRCNN [35] to perceive the objects’ velocities and positions. The input to the neural networks is a pair of images, and we compute the positions and velocities of objects appearing in the images.

At each time step, we need two consecutive frames to calculate the instantaneous velocities. Assume that the current time step is t_1 and the previous time step is $t_0 < t_1$. From the RGB camera we have two pairs of RGB images $\mathbf{I}_{t_1}, \mathbf{I}_{t_0} \in \mathbb{R}^{h \times w \times 3}$, where h, w is the height and width of the images in pixels. For simplicity, we omit t in the subscripts. The input to the FlowNet is the RGB pair $\mathbf{I}_1, \mathbf{I}_0$, and the output is the optical flow $\mathbf{O} \in \mathbb{R}^{h \times w \times 2}$, which represents the displacement of pixels in the 2D images. Therefore, one pixel $\mathbf{s}_1 = [x_1, y_1]$ in \mathbf{I}_1 corresponds to $\mathbf{s}_0 = [x_0, y_0] = [x_1 + \mathbf{O}(x_1, y_1, 1), y_1 + \mathbf{O}(x_1, y_1, 2)]$ in \mathbf{I}_0 . Assume the Lidar sequence is $\mathbf{L} = [l_1, l_2, \dots, l_k]$, where l_i is the distance to the nearest point at angle θ_i . The positions of those points in the horizontal plane can then be computed using $(l \sin \theta, l \cos \theta)$ and projected into the image space as a depth image \mathbf{D} . The depth \mathbf{D}'_0 and position \mathbf{S}'_0 of pixels in the \mathbf{I}_1 frame at t_0 time can be computed using optical flow warping [33].

The next step is to separate moving obstacles such as pedestrians from the raw image so that we can compute their positions and velocities. We feed image \mathbf{I}_1 to another segmentation network MaskRCNN to estimate pixel-level segmentation. Assume that for an object i , MaskRCNN predicts its segmentation mask $\mathbf{M}_i \in \{0, 1\}^{h \times w}$. The depth d_i and the position $\mathbf{s}_i = (x_i, y_i)$ in the image space of an object can be calculated as the weighted mean in the masked area. Let the camera have principal point $[c_x, c_y]$ and focal lengths (f_x, f_y) . The 3D position of the object can be computed as $\mathbf{p}_i = [(x_i \cdot d_i - c_x \cdot d_i) / f_x, (y_i \cdot d_i - c_y \cdot d_i) / f_y, d_i]$. After that, the relative velocities in the robot frame can be easily computed as $\bar{v}v_i = (\mathbf{p}_{1i} - \mathbf{p}_{0i}) / (t_1 - t_0)$. The

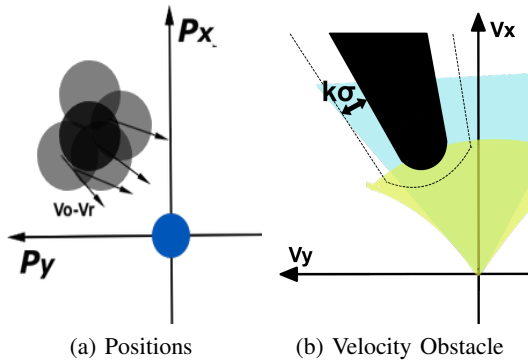


Fig. 3. Modified Velocity Obstacles algorithm for partial observation of obstacles. (a): In a given frame, the blue circle is the robot with radius r_r and velocity \mathbf{v}_r . The black area corresponds to one obstacle with the Minkowski sum of radius $r_o + r_r$, with relative velocity $\mathbf{v}_o - \mathbf{v}_r$. (b): The velocity obstacle is the black area and its nearby area within distance $k\sigma$, which is used in our probability collision avoidance. We give a bound on the confidence based on the parameter k in Section V-A. The blue area is the field-of-view of the camera. The green area is computed based on kinematic constraints of the robot. During each step, the robot has to choose one feasible velocity in the intersection of the blue and green areas, while keeping $k\sigma$ away from the black region.

corresponding absolute velocities \mathbf{v}_i can be computed from $\bar{v}v_i$ and the instantaneous velocity of the robot. Moreover, the sizes of moving obstacles appearing in the image can be estimated from the bounding box estimated using MaskRCNN. Lidar data can further compute the radius of obstacles that are outside the camera’s FOV. Compared to tracking-based velocity estimation, our method utilizes pixel-level motion information. Thus, our approach does not suffer from correspondence or loss of tracking target. Moreover, our FlowNet and MaskRCNN can take advantage of pre-trained models, which are trained on large-volume datasets and are able to generalize well to the real world as well as the simulated environments (see Fig. 5).

V. COLLISION AVOIDANCE

After detecting nearby obstacles using our perception algorithm, our navigation algorithm takes into account the uncertainty of perception, the constraint of partial observation, and kinematic constraints of the robot.

A. Probabilistic Collision Avoidance

We first account for the sensor errors and derive bounds for probabilistic collision avoidance. To accomplish this goal, we model obstacles’ parameters as Gaussian distributions and compute the velocity constraints for the robot. Our formulation uses a parameter k in Lemma 1.1, which is used to guarantee the confidence in collision avoidance.

Our bound derivation makes some assumptions on the motion of dynamic obstacles, which mostly correspond to pedestrians. We assume that there would be no large or sudden change in the velocity of the pedestrians that are in close proximity to the robot. In addition, the pedestrians will not intentionally run into a robot from behind, even though they are not in the field-of-view of the robot sensors.

Our approach builds on prior techniques based on reciprocal velocity obstacles [4], [3]. Given the position \mathbf{p}_o and velocity \mathbf{v}_o of an obstacle with radius r_o , let the robot’s

position be \mathbf{p}_r , velocity \mathbf{v}_r , and radius r_r . The velocity obstacle defined as Equation 1.

$$V_{r|o}^T = \{\mathbf{v} | \exists t \in [0, T] :: t\mathbf{v} \in D(\mathbf{p}_o - \mathbf{p}_r, r_r + r_o)\} \quad (1)$$

$$D(\mathbf{p}, r) = \{\mathbf{q} | \|\mathbf{q} - \mathbf{p}\| < r\},$$

where D is the circular disk centered at position \mathbf{p} with radius r . Because of the inaccuracies and uncertainties in real-world measurements, we assume the observed obstacles have errors in positions and velocities with different probabilities. In our formulation, the positions and velocities of obstacles are represented by Gaussian distributions, as shown in Figure 3, where gray circles are obstacles with potential positions and the arrows correspond to the potential velocities. We assume each vector is isotropic in all directions, the elements in the same vector are independent and their variances have the same relationship with respect to the distance:

$$\mathbf{p}_i \approx \mathcal{N}_2(\mu_p, \Sigma_p(d)) \quad (2)$$

$$\mathbf{v}_i \approx \mathcal{N}_2(\mu_v, \Sigma_v(d)), \mathbf{v}_r \approx \mathcal{N}_2(\mu_r, \Sigma_r), \quad (3)$$

where \mathbf{p}_i is the relative position of the i_{th} obstacle with respect to the robot; \mathbf{v}_i is the velocity of the i_{th} obstacle; d is the distance between the obstacle and the robot, and \mathbf{v}_r is the velocity of the robot. If the obstacle is near the robot, the perception errors in the position and velocity are lower. Based on the formulations, $\Sigma_v(d) = \sigma_v(d)^2 \mathbf{I}$ and $\Sigma_p(d) = \sigma_p(d)^2 \mathbf{I}$, we observe that $\sigma_v(d)^2$ and $\sigma_p(d)^2$ are monotonically decreasing.

Given a velocity of the robot \mathbf{v} and $t \in (0, T]$, let’s consider the velocity obstacle formulation given by Equation 1. In this case, we can write the constraint for velocity regions using Equation 4 as:

$$f_i(\mathbf{v}, t | \mathbf{p}_i, \mathbf{v}_i) = \|\mathbf{p}_i - (\mathbf{v} - \mathbf{v}_i)t\|^2 - (r_r + r_i)^2$$

$$f_i(\mathbf{v}, t, \mathbf{p}_i, \mathbf{v}_i) > 0, \quad (4)$$

where r_r and r_i are the radius of the robot and the obstacle i , respectively. \mathbf{v} and \mathbf{v}_i represents the velocity of the robot and the i_{th} obstacle at time t , respectively. This formulation ensures that the distance between the robot and the obstacle during the next time step is larger than the sum of their individual radius [41]. We use the following theorem about its distribution.

Theorem 1: For any velocity \mathbf{v} of the robot, the distribution of f_i , $\mathcal{D}(f_i(\mathbf{v} | \mathbf{p}_i, \mathbf{v}_i))$ is a non-central χ^2 distribution with different σ , where the mean is a function of \mathbf{v} and variance with regards to d is monotonically decreasing. d corresponds to the distance from the obstacle to the robot and is determined when the obstacle is detected.

The proof of Theorem 1 is given in Section IX in [42]. Theorem 1 highlights the property of constraints of the velocity space based on the probabilistic velocity obstacle formulation.

The variables in Equation 4 are all random variables. At time step t , we use the chance constraint $P(f_i(\mathbf{v}, t | \mathbf{p}_i, \mathbf{v}_i) > 0)$ to represent the probability of $f_i(\cdot) > 0$ in Equation 4. We denote the function $P(f_i(\mathbf{v} | \mathbf{p}_i, \mathbf{v}_i, t) > 0)$ as $P(\mathbf{v} | \mathbf{p}_i, \mathbf{v}_i, t)$. Let μ_f and σ_f denote the mean and standard deviation of the

distribution given by $f(\cdot)$, respectively. For a given $k > 0$, we enforce the distribution to have $\mu_f \pm k\sigma_f > 0$. Then, $P(\mathbf{v}|\mathbf{p}_i, \mathbf{v}_i, t)$ will increase as k gets larger. The lower bound on the probability is given by Lemma 1.1:

Lemma 1.1: Choose a scalar value $k > 0$, and let $\mu_f \pm k\sigma_f > 0$, then the chance constraint $P(\mathbf{v}|\mathbf{p}_i, \mathbf{v}_i, t)$ is lower bounded by $\frac{k^2}{1+k^2}$.

The proof of Lemma 1.1 is given in Section IX in [42]. In practice, our approach can be rather conservative when k is large. In order to guarantee collision avoidance, for all $\tau \in (0, t]$, the robot's velocity needs to satisfy $P(f_i(\mathbf{v}, \tau|\mathbf{p}_i, \mathbf{v}_i) > 0) > \frac{k^2}{1+k^2}$. As shown in Figure 3 (b), if we choose a velocity outside of $k\sigma_f$ distance of the black velocity obstacle area, the confidence of the collision avoidance is bounded by Lemma 1.1.

In this manner, we can combine the constraints formulated using all nearby obstacles. We use the function $g(\mathbf{p}_i, \mathbf{v}_i, t)$ to represent the feasible velocity area related to the obstacle i . Assume that the set C_o contains all the detected obstacles, the feasible velocities can be computed by applying all the constraints from nearby obstacles, as following equation:

$$\mathcal{G} = \bigcap_{i \in C_o} g(\mathbf{p}_i, \mathbf{v}_i). \quad (5)$$

When we choose a feasible velocity from \mathcal{G} , It is guaranteed (according to Lemma 1.1) that the confidence of collision avoidance is at least $\frac{k^2}{1+k^2}$.

B. Partial Observations

In our model, the largest robot's field-of-view is limited by the field-of-view of the 2D Lidar. For areas inside the range of the camera, the probabilistic VO formulation described above is directly used based on the information about detected obstacles. We define the area of feasible velocities as $V_c^t = \mathcal{G}$, at time step t .

Since the field-of-view of the camera is typically smaller than that of the Lidar, dynamic obstacles may appear in the detection area of this Lidar but not in the field-of-view of the RGB camera. As a result, the velocities of such obstacles are unknown and there could be potential collision during the time step t . We use additional constraints to prevent such collisions. Our approach considers two types of dynamic obstacles: robot-like obstacles and pedestrian obstacles. The robot-like obstacles have the same configurations as the robot, and pedestrian obstacles correspond to moving pedestrians, other dynamic objects, etc.

For robot-like obstacles, if we can ensure that the robot's position during the next step will lie within the field-of-view of its camera, the robots will not collide with each other since they will avoid collisions with the obstacles within their FOV of camera. This constraint is expressed as:

$$V_c = \left\{ (v_x, v_y) \mid \left| \arctan(v_y, v_x) \right| < \frac{FOV_c}{2} \right\}, \quad (6)$$

where FOV_c is the field-of-view of the camera and (v_x, v_y) are allowable velocities of the robot.

For pedestrian-obstacles we assume that there will be no sudden changes in the velocity near the robot at position \mathbf{p}_o .

Let the velocity of the obstacle be \mathbf{v}_o . We set the magnitude of velocity $\|(\mathbf{v}_o)\| = 1.5m/s$, which is the average speed of pedestrians in normal circumstances [43]. This value can change in different conditions. In order to avoid collisions, the robot needs to maintain a sufficient distance from each obstacle during the next time step. Considering the pedestrians which are out of the field-of-view of the robot's camera, the allowable velocity space is given by:

$$V_l^t = \{ \mathbf{v} \mid \|(\mathbf{v} - \mathbf{v}_o) * \tau - \mathbf{p}_o\| > C \}, \text{ for all } \tau \in (0, t], \quad (7)$$

where C is the threshold of collision (i.e. the minimum distance between the obstacle and the robot) and t is the time step.

Adding the constraints from partially-observed obstacles, the feasible velocities space is

$$V_p^t = V_c^t \bigcap V_l^t. \quad (8)$$

When calculating V_l^t , the potential velocity obstacles are conservative and have larger areas. As a result, V_l^t is smaller than that computed using the actual sizes of obstacles. If the field-of-view of the camera is larger, we can detect more potential obstacles and their velocities. In this case, V_l^t would be larger and V_p^t would also be larger.

C. Kinematic Constraints

The output of our velocity obstacle algorithm is computed using the Euclidean coordinates. In order to satisfy the kinematic constraints of the robot, we project the kinematic constraints in the Euclidean space, which is shown as the green area in Figure 3(b).

Let V_k^t denote the area computed using the kinematic constraints. As a result, the overall constraints can be represented as $V^t = V_p^t \bigcap V_k^t$. At each step, the robot has a preferred velocity of \mathbf{v}_{pref} , which is calculated according to its current position and goal position [4]. In our approach, we choose the best velocity, which is nearest to the preferred velocity from the feasible velocity space, V^t . As shown in Equation 9, we choose the velocity with the minimum L .

$$L = \arg \min_{\mathbf{v}} \|\mathbf{v} - \mathbf{v}_{\text{pref}}\|, \quad \mathbf{v} \in V^t. \quad (9)$$

VI. BENCHMARK AND RESULTS

The velocity estimation is more accurate for nearby obstacles, and the inaccuracy in position estimation increases based on the distance from the robot. more details are provided in appendix X of the paper [42]. In this section, we describe the implementation details and highlight the performance of our approach in real-world and simulated scenarios. We also highlight the improvement in the performance of our approach in scenarios with partial observations.

A. Experimental Setup

In the implementations, we use Turtlebot2 as the robot platform with one camera and one Lidar. We use Astra Orbecc camera with 70-degree field-of-view and 640×480 resolution. The Lidar is Hokuyo 2D Lidar with 240-degree field-of-view and 512 samples. We also use Pozyx to localize

target relative position to the robot. For computation we use a laptop with an Intel i7-9750H CPU (2.6 GHz) with 32 GB memory and an Nvidia GeForce RTX 2070 GPU. We run our system using Ubuntu 18.04 and ROS Melodic. The segmentation network (MaskRCNN) corresponds to mask-RCNN from detectron2 [36], and the optical flow (OFNet) network corresponds to FlowNet2 [33].

The underlying simulator used to evaluate our results is Gazebo 9.0.0, with models of Jackal and Turtlebot robots. In the simulated environments, we compare the performance DRL, DWA, and PRVO with our approach. DRL is trained by the scenarios described in [14], and DWA implementation is from the ROS package, *dwa_local_planner*. For these two approaches, the inputs correspond to Lidar data. PRVO implementation is based on [10]. Since PRVO and DWA use many parameters, we tuned them to achieve the highest success rate for each scenario. Since PRVO does not have its perception module, we use ours described in Section IV. PRVO does not consider partial observations, so it treats obstacles in the partially observed area (i.e., out of the field-of-view of the camera) as static obstacles.

B. Simulated and Real-world Scenarios

In the simulation, we create different scenarios (as shown in Figure 5) to evaluate the performance of our approach and compare with other methods, in Table I.

1. **Empty** (Figure 5(a)): In this scenario, OF-VO is tested with random goals and start positions. It is used to test if the robot has the basic functionality to go to the goal position.

2. **Static** (Figure 5(b)): This scenario requires the robot to go around static obstacles and reach the goal position.

3. **Dynamic** (Figure 5(c)): In this scenario, there is a crowd of pedestrians moving towards the robot from the front. Pedestrians do not intentionally avoid robots. Instead, the robot needs to avoid the pedestrians and find its way to the goal position.

4. **Cross** (Figure 5(d)): In this scenario, pedestrians move towards the robot from the sides. This scenario requires the robot to avoid dynamic obstacles from both sides and deal with the issues of partial observation and uncertainties.

5. **Social Behavior** (Figure 5(e)): In this scenario, pedestrians tend to follow social constraints [13]. This scenario evaluates the ability of the robot avoiding pedestrians that exhibit human-like social behaviors.

In order to fill the gap between sim-to-real we tested the approach in the real world. Figure 4 shows the implementations in four scenarios, where pedestrians are (a) standing still, (b) moving towards the robot, (c) moving between obstacles, and (d) moving in a perpendicular direction.

C. Results of Our Approach

In Table I and Table II, we highlight the performance that is generated from 200 runs in each scenario.

1) *Results of partial-observation*: Because of the limitation of sensors, we have partial observations of the obstacles around the robot. In order to evaluate the performance of different navigation algorithms, we use Scenario 5(d)

to evaluate collision avoidance performance from partially observed obstacles. In this scenario, pedestrians walk towards the robot from the left and the right sides of the robot.

As table I shows, our approach has the best performance in avoiding collisions from outside of the view of its camera. The success rate using our approach with $k = 1$ is 80%. However, for PRVO the success rate is around 60%. According to Table I, DWA does not work well in the crossing scenario. DRL is better because it uses Lidar data for perception, but cannot avoid all obstacles. These results highlight the benefits of our approach.

The performance of our algorithm improves by 33% in the crossing scene, where pedestrians may walk towards the robot from outside the field-of-view of the camera.

2) *Results of Collision Avoidance*: We compare our algorithm (OF-VO) with two other collision avoidance methods, the Dynamic-Window Approach (DWA) and a Deep Reinforcement Learning-based (DRL) approach[14]. We compare these three algorithms using three criteria:

Trajectory Length: This value gives information about the performance of each algorithm; the shortest length indicates better accuracy in terms of planning and perception.

Navigation Time: This value shows how long each algorithm takes to navigate the robot towards the goal. It gives information about the processing speed and the time taken by the navigation algorithm.

Success Rate: This value shows the percentage of the successful cases in 200 runs without collision in each scenario.

Results in Table I indicate that our method has the highest success rate in terms of avoiding collisions. DWA and DRL exhibit similar performance in the static scenario. In dynamic scenarios, DWA and DRL are more likely to collide with the pedestrians. However, the DRL method performs better than DWA because DRL also considers dynamic obstacles in training. Because of the advantages of learning based algorithms, DRL exhibits better optimality in terms of running time. As compared with DWA and DRL, our method tends to be more conservative in terms of avoiding collisions. We highlight the differences between our approach and PRVO [10] in Section VIII of [42]. Compared with PRVO [10], our method has a higher success rate, smaller trajectory length, and takes less time in terms of reaching the goal position. PRVO doesn't work well in in dynamic and cross scenarios (Fig. 5(d)). As the complexity of the scenario increases in terms of number of pedestrians, the difference in the trajectory length (and time) between our approach and PRVO increases. Overall, PRVO is more conservative than our approach, and we observe better navigation performance using our approach.

Table II shows that with a higher value of k , the success rate is higher because the confidence of collision avoidance is higher. However, with a higher value of k , the trajectory length is longer, because the robot tends to be more conservative and tries to maintain a larger distance from obstacles.

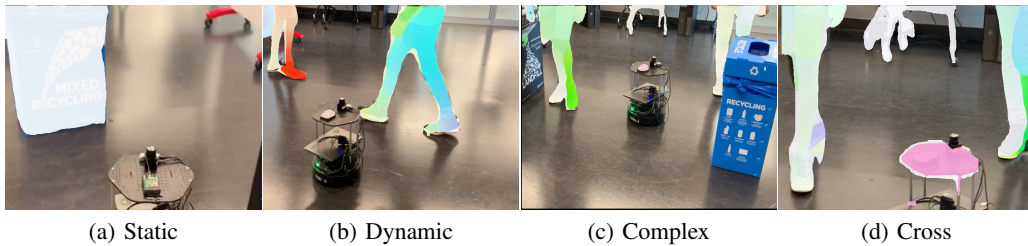


Fig. 4. Navigation across a room with different configurations: Our algorithm running on Turtlebot2 is used to navigate the robot and avoid collisions with the pedestrians and obstacles. Our algorithm can compute collision-free trajectories for the robot in these scenarios with static obstacles and multiple moving pedestrians.

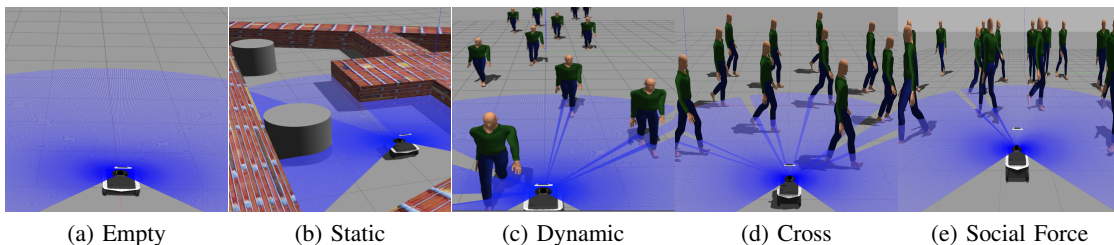


Fig. 5. Simulation Scenarios: We use six scenarios to evaluate our algorithm and analyze the performance. The scenes corresponding to (c) and (d) are dynamic scenes with multiple pedestrians. In scenario (e), pedestrians follow the social behavior [13]. The robot moves from a start point to a goal point while avoiding static and dynamic obstacles.

Scenarios	Trajectory length (m)				Navigation Time (sec)				Success Rate (%)			
	OF-VO	DWA	DRL	PRVO	OF-VO	DWA	DRL	PRVO	OF-VO	DWA	DRL	PRVO
Empty	11.3	10.7	11.1	11.2	11.7	11.6	11.5	11.8	100	100	100	100
Static obstacles	11.4	12.2	10.9	11.75	13.08	14.6	11.31	14.28	100	95	90	100
Dynamic obstacles	33.2	24.1	20.2	39.5	65.56	42.7	38.6	74.3	90	20	55	71
Cross Scenario	10.9	N/A	8.3	13.8	14.93	N/A	10.0	19.26	80	N/A	20	60
Social Behavior	12.33	11.9	10.6	14.7	18.1	14.2	12.3	25.22	92	25	70	79

TABLE I. We compare OF-VO with DWA [2] and DRL-based algorithm [14] in terms of accuracy, speed, and reliability in the simulated scenarios (Fig. 5). The number and movement of pedestrians is generated using different models, including social behavior [13] in the last row. OF-VO has the highest success rate, especially in highly dynamic environments that include dynamic obstacles and crossing scenarios. DWA and DRL result in collisions with the pedestrians, when the pedestrians' density and velocities increase.

Success Rate(%) / time(s)	k=0.1	k=0.7	k=1	k=2
Dynamic obstacles	60/22.90	76/45.67	90/65.56	97/101.40
Cross obstacles	16/10.1	64/11.51	80/14.93	83/23.67
Social Behavior	57/10.13	79/16.62	92/18.1	96/33.93

TABLE II. Success rate and running time with different values of k in our approach. The table shows that when the confidence of collision avoidance is higher, the successful rate is higher. However, with higher confidence of collision avoidance, the navigation algorithm tends to be more conservative, and this results in longer time to reach the goal.

VII. CONCLUSIONS AND LIMITATIONS

In this paper, we present a hybrid navigation algorithm that combines learning-based perception and model-based collision avoidance. We have implemented OF-VO on a Turtlebot with commodity visual sensors, including an RGB camera and a Lidar. We have evaluated the performance in complex dynamic scenes with multiple pedestrians and highlighted the benefits over prior model-based (DWA) and learning-based (DRL) methods in terms of success rate and reliability.

Although our method performs well in our benchmarks, it has some limitations. In particular, the Velocity-Obstacle is a local navigation method, and the robot is constrained so that it does not move backward. As a result, the robot may get

stuck in an impasse, where there is no feasible velocity (i.e. freezing behavior). Moreover, the optical flow estimation has lower accuracy for large displacements in the obstacles. We currently model the sensor errors using a simple Gaussian mixture model formulation, though it can be extended to other non-Gaussian noise distributions [44]. Another limitation is that our formulation can be conservative or could result in collisions if there are fast-moving obstacles outside the field-of-view of the camera. Our approach directly computes the speed of the robot without considering much about the continuity of the velocities, which leads to some jerky motions in real-world cases. As part of future work, we would like to overcome these limitations and combine our work with global navigation methods. We would also like to evaluate the performance in complex and outdoor scenes with varying number of pedestrians and relax the assumptions on pedestrian motion. In real world scenarios the pedestrian movement is governed by various constraints, including social and cultural factors, and we would like to handle such scenarios.

REFERENCES

- [1] H. Ma, S. Koenig, N. Ayanian, L. Cohen, W. Hönig, T. Kumar, T. Uras, H. Xu, C. Tovey, and G. Sharon, "Overview: Generalizations

- of multi-agent path finding to real-world scenarios,” [arXiv preprint arXiv:1702.05515](#), 2017.
- [2] D. Fox, W. Burgard, and S. Thrun, “The dynamic window approach to collision avoidance,” *IEEE Robotics & Automation Magazine*, vol. 4, no. 1, pp. 23–33, 1997.
 - [3] P. Fiorini and Z. Shiller, “Motion planning in dynamic environments using velocity obstacles,” *The International Journal of Robotics Research*, vol. 17, no. 7, pp. 760–772, 1998.
 - [4] J. Van Den Berg, S. J. Guy, M. Lin, and D. Manocha, “Reciprocal n-body collision avoidance,” in *Robotics research*. Springer, 2011, pp. 3–19.
 - [5] A. Levy, C. Keitel, S. Engel, and J. McLurkin, “The extended velocity obstacle and applying orca in the real world,” in *2015 IEEE International Conference on Robotics and Automation (ICRA)*. IEEE, 2015, pp. 16–22.
 - [6] M. Li, R. Jiang, S. S. Ge, and T. H. Lee, “Role playing learning for socially concomitant mobile robot navigation,” *CAA Transactions on Intelligence Technology*, vol. 3, no. 1, pp. 49–58, 2018.
 - [7] A. J. Sathyamoorthy, J. Liang, U. Patel, T. Guan, R. Chandra, and D. Manocha, “Densecavoid: Real-time navigation in dense crowds using anticipatory behaviors,” [arXiv preprint arXiv:2002.03038](#), 2020.
 - [8] M. Pfeiffer, M. Schaeuble, J. Nieto, R. Siegwart, and C. Cadena, “From Perception to Decision: A Data-driven Approach to End-to-end Motion Planning for Autonomous Ground Robots,” [arXiv e-prints](#), p. arXiv:1609.07910, Sep 2016.
 - [9] Y. Zhu, R. Mottaghi, E. Kolve, J. J. Lim, A. Gupta, L. Fei-Fei, and A. Farhadi, “Target-driven Visual Navigation in Indoor Scenes using Deep Reinforcement Learning,” [arXiv e-prints](#), p. arXiv:1609.05143, Sep 2016.
 - [10] B. Gopalakrishnan, A. K. Singh, M. Kaushik, K. M. Krishna, and D. Manocha, “Prvo: Probabilistic reciprocal velocity obstacle for multi robot navigation under uncertainty,” in *2017 IEEE/RSJ International Conference on Intelligent Robots and Systems (IROS)*, Sep. 2017, pp. 1089–1096.
 - [11] J. S. Park, C. Park, and D. Manocha, “Efficient probabilistic collision detection for non-convex shapes,” in *2017 IEEE International Conference on Robotics and Automation (ICRA)*. IEEE, 2017, pp. 1944–1951.
 - [12] M. Shiomi, F. Zanlungo, K. Hayashi, and T. Kanda, “Towards a socially acceptable collision avoidance for a mobile robot navigating among pedestrians using a pedestrian model,” *International Journal of Social Robotics*, vol. 6, no. 3, pp. 443–455, 2014.
 - [13] A. Bera, T. Randhavane, R. Prinja, and D. Manocha, “Sociosense: Robot navigation amongst pedestrians with social and psychological constraints,” in *2017 IEEE/RSJ International Conference on Intelligent Robots and Systems (IROS)*. IEEE, 2017, pp. 7018–7025.
 - [14] T. Fan, P. Long, W. Liu, and J. Pan, “Fully distributed multi-robot collision avoidance via deep reinforcement learning for safe and efficient navigation in complex scenarios,” [arXiv preprint arXiv:1808.03841](#), 2018.
 - [15] H. Bai, S. Cai, N. Ye, D. Hsu, and W. S. Lee, “Intention-aware online pomdp planning for autonomous driving in a crowd,” in *2015 IEEE International Conference on Robotics and Automation (ICRA)*, May 2015, pp. 454–460.
 - [16] D. Wolinski, S. J. Guy, A.-H. Olivier, M. Lin, D. Manocha, and J. Pettré, “Parameter estimation and comparative evaluation of crowd simulations,” in *Computer Graphics Forum*, vol. 33, no. 2. Wiley Online Library, 2014, pp. 303–312.
 - [17] S. Kim, S. J. Guy, W. Liu, D. Wilkie, R. W. Lau, M. C. Lin, and D. Manocha, “Brvo: Predicting pedestrian trajectories using velocity-space reasoning,” *The International Journal of Robotics Research*, vol. 34, no. 2, pp. 201–217, 2015.
 - [18] Z. Forootaninia, I. Karamouzas, and R. Narain, “Uncertainty models for ttc-based collision-avoidance,” in *Robotics: Science and Systems*, vol. 7, 2017.
 - [19] N. E. Du Toit and J. W. Burdick, “Robot motion planning in dynamic, uncertain environments,” *IEEE Transactions on Robotics*, vol. 28, no. 1, pp. 101–115, 2011.
 - [20] G. Angeris, K. Shah, and M. Schwager, “Fast reciprocal collision avoidance under measurement uncertainty,” [arXiv preprint arXiv:1905.12875](#), 2019.
 - [21] L. Xie, S. Wang, A. Markham, and N. Trigoni, “Towards Monocular Vision based Obstacle Avoidance through Deep Reinforcement Learning,” [arXiv e-prints](#), p. arXiv:1706.09829, Jun 2017.
 - [22] V. Mnih, A. P. Badia, M. Mirza, A. Graves, T. Lillicrap, T. Harley, D. Silver, and K. Kavukcuoglu, “Asynchronous methods for deep reinforcement learning,” in *International conference on machine learning*, 2016, pp. 1928–1937.
 - [23] J. Schulman, F. Wolski, P. Dhariwal, A. Radford, and O. Klimov, “Proximal policy optimization algorithms,” [arXiv preprint arXiv:1707.06347](#), 2017.
 - [24] P. Henry, C. Vollmer, B. Ferris, and D. Fox, “Learning to navigate through crowded environments,” in *2010 IEEE International Conference on Robotics and Automation*. IEEE, 2010, pp. 981–986.
 - [25] R. Henschel, L. Leal-Taixé, D. Cremers, and B. Rosenhahn, “Fusion of head and full-body detectors for multi-object tracking,” in *Proceedings of the IEEE Conference on Computer Vision and Pattern Recognition Workshops*, 2018, pp. 1428–1437.
 - [26] J.-M. Li, C. W. Chen, and T.-H. Cheng, “Estimation and tracking of a moving target by unmanned aerial vehicles,” in *2019 American Control Conference (ACC)*. IEEE, 2019, pp. 3944–3949.
 - [27] V. Tchernykh, M. Beck, and K. Janschek, “Optical flow navigation for an outdoor uav using a wide angle mono camera and dem matching,” *IFAC Proceedings Volumes*, vol. 39, no. 16, pp. 590–595, 2006.
 - [28] H. Chao, Y. Gu, and M. Napolitano, “A survey of optical flow techniques for robotics navigation applications,” *Journal of Intelligent & Robotic Systems*, vol. 73, no. 1-4, pp. 361–372, 2014.
 - [29] H. Rashed, S. K. Yogamani, A. E. Sallab, P. Krizek, and M. El-Helw, “Optical flow augmented semantic segmentation networks for automated driving,” in *Proceedings of the 14th International Joint Conference on Computer Vision, Imaging and Computer Graphics Theory and Applications, VISIGRAPP 2019, Volume 5: VISAPP, Prague, Czech Republic, February 25-27, 2019*, A. Trémeau, G. M. Farinella, and J. Braz, Eds. SciTePress, 2019, pp. 165–172. [Online]. Available: <https://doi.org/10.5220/0007248301650172>
 - [30] D. Honegger, P. Greisen, L. Meier, P. Tanskanen, and M. Pollefeys, “Real-time velocity estimation based on optical flow and disparity matching,” in *2012 IEEE/RSJ International Conference on Intelligent Robots and Systems, IROS 2012, Vilamoura, Algarve, Portugal, October 7-12, 2012*. IEEE, 2012, pp. 5177–5182. [Online]. Available: <https://doi.org/10.1109/IROS.2012.6385530>
 - [31] B. K. Horn and B. G. Schunck, “Determining optical flow,” in *Techniques and Applications of Image Understanding*, vol. 281. International Society for Optics and Photonics, 1981, pp. 319–331.
 - [32] A. Dosovitskiy, P. Fischer, E. Ilg, P. Hausser, C. Hazirbas, V. Golkov, P. Van Der Smagt, D. Cremers, and T. Brox, “FlowNet: Learning optical flow with convolutional networks,” in *Proceedings of the IEEE international conference on computer vision*, 2015, pp. 2758–2766.
 - [33] E. Ilg, N. Mayer, T. Saikia, M. Keuper, A. Dosovitskiy, and T. Brox, “FlowNet 2.0: Evolution of optical flow estimation with deep networks,” in *Proceedings of the IEEE conference on computer vision and pattern recognition*, 2017, pp. 2462–2470.
 - [34] D. Sun, X. Yang, M.-Y. Liu, and J. Kautz, “Models matter, so does training: An empirical study of cnns for optical flow estimation,” [arXiv preprint arXiv:1809.05571](#), 2018.
 - [35] K. He, G. Gkioxari, P. Dollár, and R. Girshick, “Mask r-cnn,” in *Proceedings of the IEEE international conference on computer vision*, 2017, pp. 2961–2969.
 - [36] Y. Wu, A. Kirillov, F. Massa, W.-Y. Lo, and R. Girshick, “Detectron2,” <https://github.com/facebookresearch/detectron2>, 2019.
 - [37] K. Chen, J. Wang, J. Pang, Y. Cao, Y. Xiong, X. Li, S. Sun, W. Feng, Z. Liu, J. Xu, Z. Zhang, D. Cheng, C. Zhu, T. Cheng, Q. Zhao, B. Li, X. Lu, R. Zhu, Y. Wu, J. Dai, J. Wang, J. Shi, W. Ouyang, C. C. Loy, and D. Lin, “MMDetection: Open mmlab detection toolbox and benchmark,” [arXiv preprint arXiv:1906.07155](#), 2019.
 - [38] P. Wei, L. Cagle, T. Reza, J. Ball, and J. Gafford, “Lidar and camera detection fusion in a real-time industrial multi-sensor collision avoidance system,” *Electronics*, vol. 7, no. 6, p. 84, 2018.
 - [39] J. Redmon and A. Farhadi, “Yolo9000: better, faster, stronger,” in *Proceedings of the IEEE conference on computer vision and pattern recognition*, 2017, pp. 7263–7271.
 - [40] C. Debeunne and D. Vivet, “A review of visual-lidar fusion based simultaneous localization and mapping,” *Sensors*, vol. 20, no. 7, p. 2068, 2020.
 - [41] D. Manocha, “Solving polynomial equations,” *Applications of Computational Algebraic Geometry: American Mathematical Society Short Course, January 6-7, 1997, San Diego, California*, vol. 53, p. 41, 1998.
 - [42] J. Liang, Y.-L. Qiao, T. Guan, and D. Manocha, “Of-vo: Reliable navigation among pedestrians using commodity sensors,” 2021. [Online]. Available: <https://arxiv.org/abs/2004.10976>
 - [43] R. V. Levine and A. Norenzayan, “The pace of life in 31 countries,” *Journal of Cross-Cultural Psychology*, vol. 30, pp. 178–205, 1999.
 - [44] J. S. Park and D. Manocha, “Efficient probabilistic collision detection for non-gaussian noise distributions,” *IEEE Robotics and Automation Letters*, vol. 5, no. 2, pp. 1024–1031, 2020.
 - [45] T.-Y. Lin, M. Maire, S. Belongie, J. Hays, P. Perona, D. Ramanan, P. Dollár, and C. L. Zitnick, “Microsoft coco: Common objects in context,” in *European conference on computer vision*. Springer, 2014, pp. 740–755.

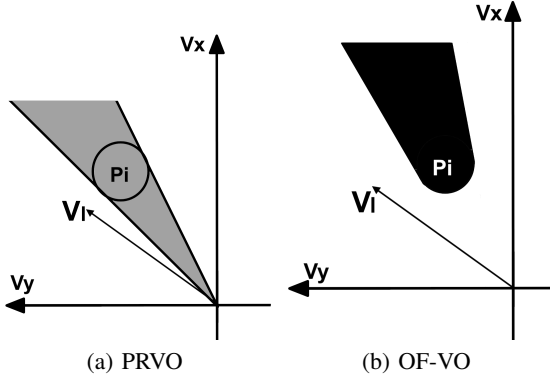


Fig. 6. In these two figures, v_i is the relative velocity of robot regarding to obstacle. p_i represents the obstacle. The velocity obstacle in our formulation is shown in the black region in (b). In contrast, the velocity obstacle space in PRVO's formulation [10] corresponds the gray space in (a). The black area is smaller than the grey one, and this means there more open space for available velocities.

Appendix

VIII. COMPARE WITH PRVO

This section talks about the differences between PRVO [10] and our approach in collision avoidance.

Our algorithm considers partial observation but PRVO does not, so when pedestrians go to two sides of the robot, PRVO is in risk to collision.

As Figure 6 shows, the black area in Figure 6 (b) is our velocity obstacle area, and the gray area in Figure 6 (a) is the velocity obstacle by PRVO. Our approach gives more accurate and smaller area of velocity obstacle of one object. Thus, there are less open space for PRVO to choose available velocities, so the PRVO is more conservative. The computation of the velocity obstacle spaces in our algorithm is given in Theorem 1.

IX. THEOREM AND LEMMA

Theorem 1: For any velocity \mathbf{v} of the robot, the distribution of f_i , $\mathcal{D}(f_i(\mathbf{v}|\mathbf{p}_i, \mathbf{v}_i))$ is a non-central χ^2 distribution with different σ , where the mean is a function of \mathbf{v} and variance with regards to d is monotonically decreasing. d corresponds to the distance from the obstacle to the robot and is determined when the obstacle is detected.

Proof: Denote $p_i = (x_i^p, y_i^p)$ with mean (μ_x^p, μ_y^p) and variance $\sigma_p(d)^2 \mathbf{I}$; $v_i = (x_i^v, y_i^v)$ with mean (μ_x^v, μ_y^v) and variance $\sigma_v(d)^2 \mathbf{I}$ and $\mathbf{v} = (v_r^x, v_r^y)$. Because \mathbf{p}_i and \mathbf{v}_i are all isotropic, we have $\mathbf{d}_{rel}(x, y)$ as the distribution of calculated points with mean μ_{rel} and variance $\Sigma_{rel}(d)$:

$$\mathbf{d}_{rel}(x, y) = \mathbf{p}_i - \mathbf{v}t + \mathbf{v}_i t \approx \mathcal{N}(\mu_{rel}, \Sigma_{rel}(d)) \quad (10)$$

$$\mu_{rel} = (\mu_{rel}^x, \mu_{rel}^y) = (\mu_x^p + \mu_x^v t - v_r^x t, \mu_y^p + \mu_y^v t - v_r^y t) \quad (11)$$

$$\Sigma_{rel}(d) = (\sigma_p(d)^2 + \sigma_v(d)^2 t^2) \mathbf{I} \quad (12)$$

According to Noncentral chi-squared distribution, the distribution of l_2 norm of \mathbf{d}_{rel} is represented as $\mathcal{X}_2^2(v|\mathbf{p}_i, \mathbf{v}_i)$, and

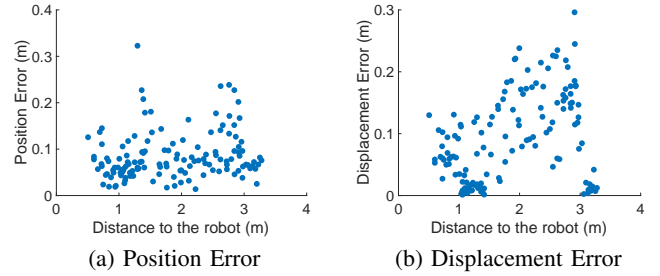


Fig. 7. Error in distance and displacement estimation: (a) shows that the errors in position estimation are distributed uniformly along the obstacles' distance. (b) shows that the errors in displacement estimation increase with the distance. The estimation has the highest accuracy at 1 meter distance.

d is the detected distance of the obstacle:

$$\mu_{norm} = 2 + (\mu_{rel}^x)^2 + (\mu_{rel}^y)^2 = k(v) \quad (13)$$

$$\sigma_{norm} = 4(\sigma_p(d)^2 + \sigma_v(d)^2 t^2)(1 + (\mu_{rel}^x)^2 + (\mu_{rel}^y)^2) = g(d) \quad (14)$$

Then we have $\mu_f(\mathbf{v}) = \mu_{norm} - (r_r + r_i)^2$ and $\sigma_f(d) = g(d)$ as mean and standard deviation of f_i . According to 14, since $\sigma_p(d)^2$ and $\sigma_v(d)^2$ are all monotonically decreasing w.r.t. d , the variance of f_i is also monotonically decreasing. ■

Lemma 1.1: Choose a scalar value $k > 0$, and let $\mu_f \pm k\sigma_f > 0$, then the chance constraint $P(\mathbf{v}|\mathbf{p}_i, \mathbf{v}_i, t)$ is lower bounded by $\frac{k^2}{1+k^2}$.

Proof: In order to satisfy the constraint function $P(f_i(\mathbf{v}|\mathbf{p}_i, \mathbf{v}_i, t) > 0)$, we can give a bound to function f_i to constraint the random variable to be positive, then we have:

$$(X - \mu_f) - k|\sigma_f| > 0 \quad (15)$$

According to Cantelli's inequality, we have:

$$P(f_i(\mathbf{v}|\mathbf{p}_i, \mathbf{v}_i, t) > 0) > \frac{k^2}{1+k^2} \quad (16)$$

■

X. ERROR ANALYSIS OF PERCEPTION NETWORKS

In this section, we analyze the errors from our perception algorithm. We estimate the position and displacement of obstacles between consecutive frames. The velocities of obstacles can be computed by the displacement, robot velocities, and time steps. We plot the L2 error of estimations in Figure 7. The results indicate that the displacement (velocity) estimation is more accurate for nearby obstacles, and the inaccuracy in position estimation increases based on the distance from the robot.

We analyze the accuracy of the two networks used in our perception algorithm. As reported by FlowNet2 [33], the average endpoint error in KITTI 2012 is $e_f = 4.09$, which means that predicted optical flows are 4.09 pixels away from the ground truth (on average). For an object with depth z , an error of e_f pixels in optical flow would result in an error of $e_f \cdot z/f$ to its displacement estimation. In our implementation, we have focal lengths $f_x = f_y = 457$, so the error for an object at $2m$ away would be $0.02m$. The

error of MaskRCNN is harder to quantify. From Figure 1, we can see that the segmentation of the pedestrian is reasonably good in our benchmarks. The average precision (.50 IoU) of MaskRCNN is 62.3% [35] on the COCO dataset [45], which means nearly two-thirds of predictions have more than .50 IoU. In order to make our collision avoidance more conservative, we enlarge the bounding box of moving obstacles by more than 50%. Since the networks we use are pre-trained on large datasets mixed with both simulation and real-world images, the sensor noise is largely covered in the training data. We did not observe a significant difference between the simulation and real performance.